Computers and Concrete, *Vol. 19, No. 2 (2017) 143-152*
DOI: https://doi.org/10.12989/cac.2017.19.2.143

Modeling of time-varying stress in concrete under axial loading and sulfate attack

Guang-Ji Yin, Xiao-Bao Zuo*, Yu-Juan Tang, Olawale Ayinde and Dong-Nan Ding

Department of Civil Engineering, Nanjing University of Science & Technology, Nanjing 210094, China

(Received June 16, 2016, Revised November 11, 2016, Accepted November 16, 2016)

Abstract. This paper has numerically investigated the changes of loading-induced stress in concrete with the corrosion time in the sulfate-containing environment. Firstly, based on Fick's law and reaction kinetics, a diffusion-reaction equation of sulfate ion in concrete is proposed, and it is numerically solved to obtain the spatial and temporal distribution of sulfate ion concentration in concrete by the finite difference method. Secondly, by fitting the existed experimental data of concrete in sodium sulfate solutions, the chemical damage of concrete associated with sulfate ion concentration and corrosion time is quantitatively presented. Thirdly, depending on the plastic-damage mechanics, while considering the influence of sulfate attack on concrete properties, a simplified chemo-mechanical damage model, with stress-based plasticity and strain-driven damage, for concrete under axial loading and sulfate attack is determined by introducing the chemical damage degree. Finally, an axially compressed concrete prism immersed into the sodium sulfate solution is regarded as an object to investigate the time-varying stress in concrete subjected to the couplings of axial loading and sulfate attack.

Keywords: time-varying stress; concrete; chemo-mechanical damage model; sulfate attack; axial loading

1. Introduction

Concrete structures, while carrying various external loads, are also subjected to chemical attack for a long period in sulfate-containing environments (Gao *et al.* 2013, Yang *et al*. 2005). Sulfate ions in environment diffuse into concrete and react with the cement hydration products to generate expansive crystals such as gypsum and ettringite (Taylor *et al.* 2001). The growth of these crystals in concrete pores will cause chemical damage, such as volumetric expansion, cracking and spalling, which finally leads to the degradation of concrete properties (Idiart *et al.* 2011, Kalipcilar *et al.* 2016, Neville 2004). Furthermore, the stresses from the applied loads result in the extension of micro-cracks in concrete, which not only create the mechanical damage, but also change the transport mechanism (Sun and Zuo 2012a), and accelerates the transport of sulfate ions and chemical damage of concrete under sulfate attack (Bassuoni and Nehdi 2009, Gao *et al.* 2013, Xiong *et al.* 2015).

The chemical damage of concrete in sulfate-containing environment is a complex physico- chemical deterioration process, which involves the transport of sulfate ions, microstructure damage and degradation of macro-mechanical properties (Güneyisi *et al.* 2010, Yu *et al.* 2015). Some researchers have carried out many corrosion experiments to investigate the transport of sulfate ions in concrete specimens immersed into sulfate solution with different concentrations, and applied EDTA titration method to quantitatively analyze the distribution of sulfate ions in the specimens (Sun *et al.* 2013, Zuo *et al.* 2012a). In order to numerically analyze its transport mechanism, a diffusion model of sulfate ions in concrete was developed using Fick's law (Nie *et al.* 2015, Samson and Marchand 2007, Sun *et al.* 2013). Based on SEM and CT microscopic observation on the concrete sample of corrosion experiments, the influence of sulfate concentration on the damage process of concrete was investigated (Nehdi *et al.* 2014, Yuan *et al.* 2016), and the evolution of its microstructure, caused by the growth of gypsum and ettringite crystals, was also studied to obtain the damage mechanism of concrete (Liu *et al.* 2012a, Santhanam *et al.* 2003). Through the experiments on the mechanical properties of corroded Portland cement concrete, the changes of concrete properties with corrosion time, such as strength and elastic modulus, were analyzed to obtain the whole stress-strain curve associated with sulfate concentration and corrosion time (Liu *et al.* 2012b, Liang and Yuan 2005, Schneider and Chen 1998, Zhou *et al.* 2016).

The mechanical damage of concrete caused by external loading is another important factor influencing the long-term in-service behavior of concrete structures, and currently there are many achievements on studies in this aspect, such as the classical Mazars's damage model (Mazars and Pyaudier-Cabot 1989), Borcelona damage model (Lubliner *et al.* 1989), Faria's damage constitutive model, associated with strain-rate dependent plasticity (Faria *et al.* 1998) and Wu's plastic-damage model based on damage energy release rate (Wu *et al.* 2006). However, these models have mainly focused on modeling the damage of concrete subjected to loading actions, without considering the influence of damage caused by chemical

*Corresponding author, Ph.D.
E-mail: xbzuo@sina.com

ISSN: 1598-8198 (Print), 1598-818X (Online)

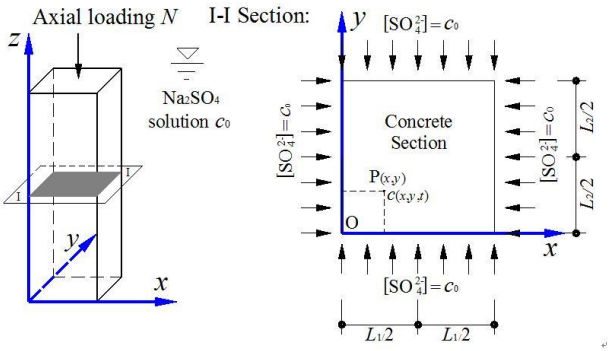

Fig. 1 Two-dimensional diffusion model of sulfate ion in concrete under axial loading

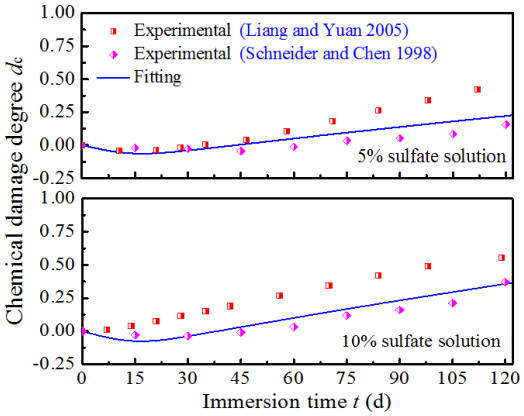

Fig. 2 The comparison of the experimental data and fitting expression in Eq. (4) for d_c

attack like sulfate, which also reduces the mechanical properties of concrete materials. In fact, the chemical damage induced by sulfate attack mainly depend on sulfate ion concentration in the concrete sample and corrosion time, having a gradient distribution from the surface to the interior, but the damage degree obtained from the corrosion experiment is just an average value, which cannot characterize the time-varying gradient distribution. So, in order to evaluate the mechanical behavior of concrete materials and structures, it is necessary to quantitatively describe a spatial and temporal chemo-mechanical damage of concrete under coupled external loading and sulfate attack.

This paper utilizes an axially compressed concrete prism with ordinary Portland cement in the sodium sulfate solution as a case study, and a quantitative description of the time-varying stress in the concrete prism section is presented. A diffusion-reaction process of sulfate ion in concrete is firstly modeled in section 2, and combining the existed experimental data, the sulfate-induced chemical damage is described. Based on the plastic-damage mechanics, a simplified chemo-mechanical damage model is adopted to analyze the time-varying stress in concrete prism in section 3. In section 4, the finite difference method with Alternating Direction Implicit (ADI) scheme is adopted for solving the diffusion model of sulfate ion, while the Euler backward algorithm are used to solve the time-varying stress in concrete. Finally, a numerical example is carried out in section 5.

2. Sulfate-induced chemical damage

2.1 Diffusion model

Under sulfate attack, the chemical damage of concrete is related to the concentration of sulfate ions in concrete (Saetta *et al.* 1998), so, modeling the diffusion process of sulfate ion is necessary for quantitative characterization of the chemical damage.

A concrete prism specimen subjected to axial load and Na_2SO_4 solution was used in this paper, as shown in Fig. 1. Due to the coexistence of ionic diffusion and chemical reaction, the diffusion process of sulfate ions in the specimen was modeled using Fick's second law and chemical reaction kinetics, and it is expressed by

$$\begin{cases} \dfrac{\partial c}{\partial t}=\dfrac{\partial\left(D_c^{\sigma}\dfrac{\partial c}{\partial x}\right)}{\partial x}+\dfrac{\partial\left(D_c^{\sigma}\dfrac{\partial c}{\partial y}\right)}{\partial y}+\dfrac{\partial C_d}{\partial t} \\ c(x,y,0)=0, \quad (x,y)\in\Omega \\ c(x,0,t)=c_0, \quad c(0,y,t)=c_0 \\ c(L_1,y,t)=c_0, \quad c(x,L_2,t)=c_0 \end{cases} \tag{1}$$

Where $c(x, y, t)$ is the sulfate ion concentration in concrete specimen; (x, y) is the location in the specimen section Ω, t represents the total corrosion time; c_0 is the concentration of sodium sulfate solution; D_c^{σ} is the diffusion coefficient of sulfate ion in concrete considering the effect of stress, and it can be referred in documents (Zuo *et al.* 2010), L_1 and L_2 are the lengths of section along x and y directions; C_d is the dissipated concentration of sulfate ion caused by chemical reaction.

In the penetration process, part of the sulfate ions react with the dissolved calcium hydroxide (CH) in the concrete pore to produce the secondary gypsum ($C\bar{S}H_2$), as shown in Eq. (2). Since the equation is a second-order chemical reaction (Nie *et al.* 2015), and based on the chemical reaction kinetics, the kinetic equation in Eq. (2), which can determine a relation between the free and dissipated concentration of sulfate ions in concrete, is expressed in Eq. (3) as

$$CH\left(Ca^{2+}+OH^{-}\right)+SO_4^{2-}\rightarrow C\bar{S}H_2+2\,OH^{-} \tag{2}$$

$$\frac{\partial C_d}{\partial t}=-k_v\cdot c_{Ca}\cdot c \tag{3}$$

Where k_v is the chemical reaction rate constant, c_{Ca} is the saturated concentration of calcium ion in the concrete pore solution.

2.2 Chemical damage degree

The results of corrosion experiments (Liang and Yuan 2005, Schneider and Chen 1998) show that the changes of

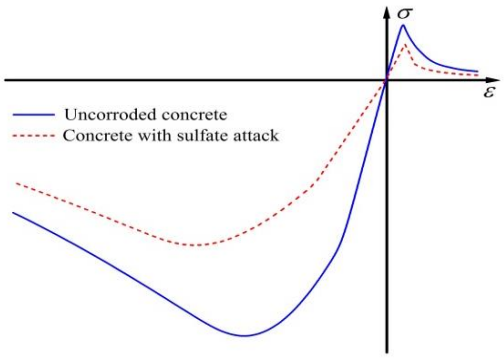

Fig. 3 Influence of sulfate attack on the concrete constitutive relation

concrete properties with sulfate concentration and corrosion time. Similar to the concept of mechanical damage in damage mechanics, the chemical damage degree is introduced to quantitatively characterize the degradation of concrete specimen caused by sulfate attack, and according to the fitting formula (Cao 1991) and the above experimental results, its expression, associated with the diffused sulfate ion concentration c and the corrosion time t_{in}, can be obtained by

$$d_c = \begin{cases} -(0.9c + 0.04)\sqrt[3]{t_{in}} + (0.0111 + 0.41c - 1.014c^2)\sqrt[3]{t_{in}^2} & c > 0 \\ 0 & c = 0 \end{cases} \quad (4)$$

Where d_c is the chemical damage degrees characterizing the degradation of concrete properties including strength, elastic modulus and ultimate strain. Fig. 2 presents the comparison of the experimental results and fitting expression in Eq. (4) for the chemical damage degree d_c.

The corrosion time t_{in} at the position (x,y) in the concrete specimen is associated with its initial corrosion moment $t_{0so}(x,y)$, which is the time needed for the sulfate ion to move from the specimen surface to the position (x,y). Based on the numerical solution of Eq. (1), the corrosion front position (x_{ch}, y_{ch}) and the corresponding time $t_{0so}(x_{ch}, y_{ch})$ can be obtained using

$$c(x,y,t)\big|_{x=x_{ch},\,y=y_{ch}} = 0, \quad \frac{\partial c}{\partial x}\left(or \frac{\partial c}{\partial y}\right)\Bigg|_{x=x_{ch},\,y=y_{ch}} \neq 0 \quad (5)$$

Where (x_{ch}, y_{ch}) refers to the sulfate-corrosion front position in concrete which varies with total immersion time t. Thus, the corrosion time t_{in} at the position (x,y) in concrete can be calculated by

$$t_{in} = t - t_{0so}(x, y) \quad (6)$$

Similar to the mechanical damage (Yu and Feng 1997), the degradation of corroded concrete caused by chemical damage, including the changes of concrete strength and elastic modulus (Sarkar *et al.* 2010), can be expressed as

$$f = [1 - d_c] \cdot f_0 \quad (7)$$

$$E = [1 - d_c] \cdot E_0 \quad (8)$$

Where f_0, E_0, and f, E are the strength and elastic modulus of uncorroded and corroded concrete.

3. Chemo-mechanical damage model

3.1 Constitutive relation with chemo-mechanical damage

The stress produced by the applied load results in the propagation of micro-cracks in concrete, which causes mechanical damage and plastic deformation (Shao *et al.* 2006). In the loading process, the evolution of mechanical damage is accompanied by the plastic deformation in concrete (Zheng *et al.* 2012). Furthermore, chemical damage caused by sulfate attack leads to the degradation of concrete properties, including elastic modulus, compressive and tensile strength. They may reduce the yield surface in the effective stress space and increase the plastic deformation of concrete under loading actions, and further accelerate the process of mechanical damage of concrete, but will not change the curve shape of concrete constitutive relation. Thus, in order to characterize the mechanical damage coupled with plastic deformation caused by loading, and meanwhile reflect the influence of sulfate corrosion, a simplified coupled chemo-mechanical damage model for concrete can be obtained by introducing the chemical damage degree. The model consists of the plastic and damaged parts described by effective stress and plastic strain respectively.

Based on the concept of effective stress and strain equivalence hypothesis, and combined with Eq. (8), the simplified constitutive relation, associated with the coupled chemo-mechanical damage, for concrete under axial loading and sulfate attack can be expressed as (Taqieddin *et al.* 2012)

$$\sigma = (1 - d_m) \cdot \bar{\sigma} = (1 - d_m) \cdot (1 - d_c) \cdot E_0 \cdot (\varepsilon - \varepsilon^p) \quad (9)$$

Where σ, $\bar{\sigma}$, ε and ε^p are the nominal stress, effective stress, total strain and the plastic strain of concrete respectively; d_m is the mechanical damage caused by the axial loading. The influence of sulfate attack on the concrete constitutive relation is shown in Fig. 3.

3.2 Plasticity model with chemical damage

According to the plasticity theory, and considering the influence of sulfate corrosion on concrete properties, a simplified plasticity model for concrete under axial loading is described by the yield function F^p, the flow rule, the evolution law for the plastic hardening variable κ^p and the loading-unloading conditions (Grassl and Jirásek 2006).

3.2.1 Yield function

From the plasticity yield characteristics of concrete under loading, the three-parameter failure criterion of

concrete (Menétry and Willam 1995) for multiaxial stress state is adopted. Thus, the yield function F^{p} for uniaxial loading is given as

$$F^{\mathrm{p}}=\begin{cases}\left[\dfrac{\bar{\sigma}}{(1-d_{\mathrm{c}})\cdot f_{\mathrm{c0}}}\right]^2-q_{\mathrm{c}}^2 & \bar{\sigma}<0\\ \left[\dfrac{\bar{\sigma}}{(1-d_{\mathrm{c}})\cdot f_{\mathrm{c0}}}\right]^2+\dfrac{\left(f_{\mathrm{c0/t0}}-f_{\mathrm{t0/c0}}\right)\cdot\bar{\sigma}}{(1-d_{\mathrm{c}})\cdot f_{\mathrm{c0}}}-1 & \bar{\sigma}>0\end{cases} \tag{10}$$

Where f_{c0} and f_{t0} are the uniaxial compressive and tensile strength of uncorroded concrete respectively, $f_{\mathrm{c0/t0}}=f_{\mathrm{c0}}/f_{\mathrm{t0}}$, $f_{\mathrm{t0/c0}}=f_{\mathrm{t0}}/f_{\mathrm{c0}}$; q_{c} is the dimensionless parameter reflecting the shape and size of yield surface in the effective stress space

$$q_{\mathrm{c}}=\begin{cases}q_{\mathrm{c0}}+\left(1-q_{\mathrm{c0}}\right)\kappa^{\mathrm{p}}\left[\left(\kappa^{\mathrm{p}}\right)^2-3\kappa^{\mathrm{p}}+3\right], & \text{if } \kappa^{\mathrm{p}}<1\\ 1, & \text{if } \kappa^{\mathrm{p}}\geq 1\end{cases} \tag{11}$$

q_{c0} is the initial equivalent compressive strength invariant

$$q_{\mathrm{c0}}=f_{\mathrm{e0}}/f_{\mathrm{c0}} \tag{12}$$

f_{e0} is the elastic limit strength of uncorroded concrete.

3.2.2 Flow rule

Based on the plastic deformation of concrete in the loading process, a non-associated plastic flow rule is adopted, and its expression can be

$$\dot{\varepsilon}^{\mathrm{p}}=\dot{\lambda}\frac{\partial G^{\mathrm{p}}}{\partial\bar{\sigma}} \tag{13}$$

Where λ is the plastic multiplier related to the increment and direction of stress, G^{p} is the plastic potential, which is given by (Etse and Willam 1999)

$$G^{\mathrm{p}}=\left[\frac{\bar{\sigma}}{(1-d_{\mathrm{c}})\cdot f_{\mathrm{c0}}}\right]^2+\left\{A_gB_g\exp\left[\frac{\bar{\sigma}-(1-d_{\mathrm{c}})\cdot f_{\mathrm{t0}}}{3B_g\cdot(1-d_{\mathrm{c}})\cdot f_{\mathrm{c0}}}\right]-\frac{\left(f_{\mathrm{c0/t0}}-f_{\mathrm{t0/c0}}\right)\cdot\bar{\sigma}}{3(1-d_{\mathrm{c}})\cdot f_{\mathrm{c0}}}\right\}\cdot q_{\mathrm{c}}^2 \tag{14}$$

A_g and B_g are expressed as

$$A_g=2f_{\mathrm{t0/c0}}+f_{\mathrm{c0/t0}}$$
$$B_g=\frac{\left(1+f_{\mathrm{t0/c0}}\right)/3}{\ln A_g-\ln\left(3+0.5f_{\mathrm{c0/t0}}-0.5f_{\mathrm{t0/c0}}\right)+0.972} \tag{15}$$

3.2.3 Evolution law of hardening variable

It can be assumed that, under uniaxial tension, concrete will produce damage when it begins the plastic deformation. Thus, the hardening variable κ^{p} is related to the length of plastic strain (Grassl *et al.* 2002), and its evolution law for concrete in the uniaxial stress state can be expressed as

$$\kappa_0^{\mathrm{p}}=\frac{1}{2}\left[\left|\mathrm{sign}\left(\bar{\sigma}\right)\right|+\mathrm{sign}\left(\bar{\sigma}\right)\right],\quad \dot{\kappa}^{\mathrm{p}}=\frac{\dot{\varepsilon}^{\mathrm{p}}}{2x^{\mathrm{p}}}\left[\mathrm{sign}\left(\bar{\sigma}\right)-\left|\mathrm{sign}\left(\bar{\sigma}\right)\right|\right] \tag{16}$$

Where k_0^p is the initial hardening variable. Sign($\bar{\sigma}$) is a symbol function, if $\bar{\sigma}>0$, sign($\bar{\sigma}$)=1, if $\bar{\sigma}<0$, sign($\bar{\sigma}$)=−1 and if $\bar{\sigma}=0$, sign($\bar{\sigma}$)=0. x^{p} is the hardening ductility, expressing the relation between $\dot{k}^p$ and $\dot{\varepsilon}^p$.

3.3 Load-induced damage model

The nonlinearity of concrete under loading indicates that its damage behaviors are different in the compressive and tensile stress states (Wu *et al.* 2006). Thus, two damage variables proposed by Mazars and Pyaudier-Cabot (1989), a tensile damage d_{mt} and a compressive damage d_{mc}, are introduced to describe the damage process of concrete under uniaxial tension and compression, and their evolution laws can be described by two damage driving variables, $\kappa_{\mathrm{t}}^{\mathrm{d}}$ for tension and $\kappa_{\mathrm{c}}^{\mathrm{d}}$ for compression.

In order to quantitatively characterize the mechanical damage caused by loading, the damage model is described by the damage loading function $F_{\varsigma}^{\mathrm{d}}$, the damage evolution law g^{d}, and the loading-unloading conditions (Grassl and Jirásek 2006).

3.3.1 Damage loading function

The mechanical damage of concrete usually occur in the direction of the maximum plastic strain (Zheng *et al.* 2012), so its damage loading function in the tensile and compressive states can be respectively described by the equivalent principal plastic strain

$$F_{\varsigma}^{\mathrm{d}}=\mathrm{sign}\left(\bar{\sigma}\right)\cdot\varepsilon^{\mathrm{p}}-\kappa_{\varsigma}^{\mathrm{d}} \tag{17}$$

Where the subscript $\varsigma=(c,t)$ is expressed as the compressive or tensile state.

According to the loading-unloading conditions ($F_{\varsigma}^{d}\leq 0$, $\dot{k}_{\varsigma}^{d}\geq 0$, $\dot{k}_{\varsigma}^{d}F_{\varsigma}^{d}=0$), it can be obtained that, when $F_{t}^{d}=0$ or $F_{c}^{d}=0$, mechanical damage occurs in concrete, so the damage driving variables $\kappa_{\mathrm{t}}^{\mathrm{d}}$ and $\kappa_{\mathrm{c}}^{\mathrm{d}}$ in Eq. (17) can be expressed as

$$\kappa_{\varsigma}^{\mathrm{d}}=\mathrm{sign}\left(\bar{\sigma}\right)\cdot\varepsilon^{\mathrm{p}} \tag{18}$$

3.3.2 Damage evolution law

Based on Mazars's damage model (Mazars and Pyaudier-Cabot 1989), the evolution law g^{d}, which is the damage variables d_{mt} and d_{mc} associated with the damage driving variables k_t^d and k_c^d and considering the influence of chemical damage d_{c}, can be expressed as

$$d_{\mathrm{m}\varsigma}=g^{\mathrm{d}}\left(\kappa_{\varsigma}^{\mathrm{d}},d_{\mathrm{c}}\right)=1-\frac{1-A_{\varsigma}}{1+\kappa_{\varsigma}^{\mathrm{d}}/\left[\left(1-d_{\mathrm{c}}\right)\cdot\varepsilon_{\varsigma 0}^{\mathrm{d}}\right]}-\frac{A_{\varsigma}}{\exp\left\{B_{\varsigma}\kappa_{\varsigma}^{\mathrm{d}}/\left[\left(1-d_{\mathrm{c}}\right)\cdot\varepsilon_{\varsigma 0}^{\mathrm{d}}\right]\right\}} \tag{19}$$

Where $\varepsilon_{\varsigma 0}^{d}$ ($\varsigma=t$, c) refers to the peak strains of uncorroded concrete when the mechanical damage occurs under uniaxial tension and compression respectively, A_{ς} and

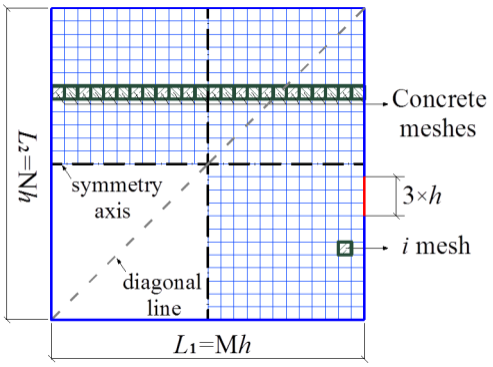

Fig. 4 Mesh of concrete prism section

B_ς are the material parameters (Mazars and Pyaudier-Cabot 1989, Wu *et al.* 2006).

3.4 Time-varying stress in concrete prism

An axially loaded concrete prism, shown in Fig. 1, is regarded as a research object to investigate the changes of stress in concrete under the axial loading and sulfate attack by using the above chemo-mechanical damage model. It can be assumed that the section of concrete prism keeps plane during the couplings of axial loading N and sulfate attack, according to the force balance in the axial direction, the stress in the cross section of concrete prism is given by

$$N = \iint_{\Omega} \sigma dxdy \tag{20}$$

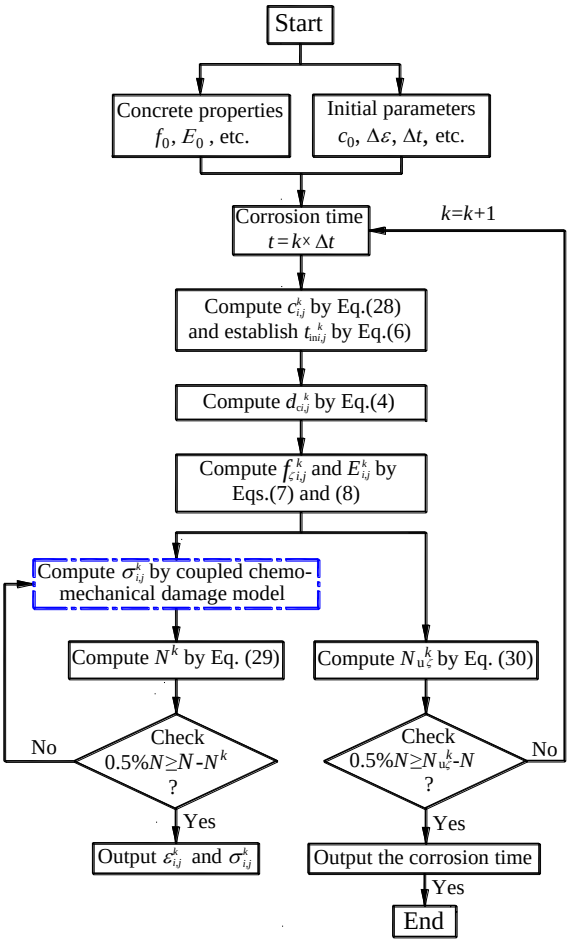

Fig. 5 Flow chart for analysis of time-varying stress in concrete

4. Numerical approach

4.1 Mesh

In order to numerically solve Eq. (1), to obtain the time-varying sulfate ion concentration in the concrete prism, the cross section of the concrete prism needs to be meshed, as illustrated in Fig. 4. The specific meshing method is that the sectional area $\Omega(L_1\times L_2)$ of the prism is meshed with equal spacing, h, along both L_1 and L_2, so two clusters of parallel lines are defined: $x_i=ih$ (i=0, 1, 2, …, i, …, M; M is the number of grid in the x direction), $y_j=jh$ (j=0, 1, 2, …, j, …, N; N is the number of grid in the y direction). The time interval is selected as Δt, so the concentration of sulfate ion can be discrete as $t_k=k\Delta t$ (k=0, 1, …, k, …, K; K is the total number of corrosion time intervals). The sectional area $\Omega(L_1\times L_2)$ is divided into square grids (M×N), the grid nodes are (x_i,y_j,t_k), and the sulfate ion concentration at the state (x_i,y_j,t_k) is expressed by $c_{i,j}^k$.

4.2 ADI difference scheme

Eq. (1) is a nonlinear partial differential equation, and it can be solved by the finite difference method with ADI scheme, in which the transition time $t_{k+1/2}$ is used to divide the time interval $(t_k,\ t_{k+1})$ into two intervals, $(t_k,\ t_{k+1/2})$ and $(t_{k+1/2},\ t_{k+1})$. The solution of Eq. (1) was obtained by two steps to get the iterative solution of sulfate ion concentration in Eq. (1).

Firstly, at the interval $(t_k,\ t_{k+1/2})$, $\partial c/\partial x$, $\partial^2 c/\partial x^2$ and time $t_{k+1/2,}$ the implicit difference quotient is used in the x direction, but at $\partial c/\partial y$ and $\partial^2 c/\partial y^2$ and time $t_{k,}$ the explicit difference quotient is used in the y direction. So Eq. (1) can be separately expressed as

$$\frac{\partial c_{i,j}^k}{\partial t}=\frac{c_{i,j}^{k+1/2}-c_{i,j}^k}{\Delta t/2} \tag{21}$$

$$\frac{\partial}{\partial x}\left(D_c^{\sigma}\frac{\partial c_{i,j}^{k+1/2}}{\partial x}\right)=\frac{1}{h^2}\left[D_{cx_{i+1/2,j}}^{\sigma^{k+1/2}}\left(c_{i+1,j}^{k+1/2}-c_{i,j}^{k+1/2}\right)-D_{cx_{i-1/2,j}}^{\sigma^{k+1/2}}\left(c_{i,j}^{k+1/2}-c_{i-1,j}^{k+1/2}\right)\right] \tag{22}$$

$$\frac{\partial}{\partial y}\left(D_c^{\sigma}\frac{\partial c_{i,j}^{k}}{\partial y}\right)=\frac{1}{h^2}\left[D_{cy_{i,j+1/2}}^{\sigma^{k}}\left(c_{i,j+1}^{k}-c_{i,j}^{k}\right)-D_{cy_{i,j-1/2}}^{\sigma^{k}}\left(c_{i,j}^{k}-c_{i,j-1}^{k}\right)\right] \tag{23}$$

In Eqs. (22) and (23), the diffusion coefficient may be

$$\begin{cases} D_{cx_{i+1/2,j}}^{\sigma^{k+1/2}}=\frac{1}{2}\left(D_{cx_{i,j}}^{\sigma^k}+D_{cx_{i+1,j}}^{\sigma^k}\right), & D_{cx_{i-1/2,j}}^{\sigma^{k+1/2}}=\frac{1}{2}\left(D_{cx_{i-1,j}}^{\sigma^k}+D_{cx_{i,j}}^{\sigma^k}\right) \\ D_{cy_{i,j+1/2}}^{\sigma^k}=\frac{1}{2}\left(D_{cy_{i,j}}^{\sigma^k}+D_{cy_{i,j+1}}^{\sigma^k}\right), & D_{cy_{i,j-1/2}}^{\sigma^k}=\frac{1}{2}\left(D_{cy_{i,j-1}}^{\sigma^k}+D_{cy_{i,j}}^{\sigma^k}\right) \end{cases} \tag{24}$$

Placing Eqs. (3), (21)-(24) into Eq. (1), the iterative solutions of Eq. (1) at the interval (t_k,$t_{k+1/2}$) can be obtained by

$$-\frac{r}{4}\left(D_{\mathrm{cx}_{i,j}}^{\sigma^k}+D_{\mathrm{cx}_{i-1,j}}^{\sigma^k}\right)c_{i-1,j}^{k+1/2}+\left[1+\frac{r}{4}\left(D_{\mathrm{cx}_{i-1,j}}^{\sigma^k}+2D_{\mathrm{cx}_{i,j}}^{\sigma^k}+D_{\mathrm{cx}_{i+1,j}}^{\sigma^k}\right)\right]c_{i,j}^{k+1/2}-\frac{r}{4}\left(D_{\mathrm{cx}_{i,j}}^{\sigma^k}+D_{\mathrm{cx}_{i+1,j}}^{\sigma^k}\right)c_{i+1,j}^{k+1/2}$$
$$=\frac{r}{4}\left(D_{\mathrm{cy}_{i,j}}^{\sigma^k}+D_{\mathrm{cy}_{i,j-1}}^{\sigma^k}\right)c_{i,j-1}^{k}+\left[1+\frac{\Delta t}{2}J-\frac{r}{4}\left(D_{\mathrm{cy}_{i,j-1}}^{\sigma^k}+2D_{\mathrm{cy}_{i,j}}^{\sigma^k}+D_{\mathrm{cy}_{i,j+1}}^{\sigma^k}\right)\right]c_{i,j}^{k}+\frac{r}{4}\left(D_{\mathrm{cy}_{i,j}}^{\sigma^k}+D_{\mathrm{cy}_{i,j+1}}^{\sigma^k}\right)c_{i,j+1}^{k} \quad (25)$$

(i, j=1, 2, ..., M-1; k=0, 1, 2, ..., K-1)

Where the parameters r and J are

$$r=\frac{\Delta t}{h^2},\quad J=-k_{\mathrm{v}}\cdot c_{\mathrm{Ca}^{2+}} \quad (26)$$

Secondly, at the interval ($t_{k+1/2}$, t_{k+1}), $\partial c/\partial x$, $\partial^2 c/\partial x^2$ and time $t_{k+1/2}$, the explicit difference quotient is used in the x direction, but for $\partial c/\partial y$ and $\partial^2 c/\partial y^2$ at the time t_{k+1}, the implicit difference quotient is used in the y direction. Likely, the iterative solutions of Eq. (1) at the interval ($t_{k+1/2}$, t_{k+1}) can be

$$-\frac{r}{4}\left(D_{\mathrm{cy}_{i,j}}^{\sigma^k}+D_{\mathrm{cy}_{i,j+1}}^{\sigma^k}\right)c_{i,j+1}^{k+1}+\left[1+\frac{r}{4}\left(D_{\mathrm{cy}_{i,j-1}}^{\sigma^k}+2D_{\mathrm{cy}_{i,j}}^{\sigma^k}+D_{\mathrm{cy}_{i,j+1}}^{\sigma^k}\right)\right]c_{i,j}^{k+1}-\frac{r}{4}\left(D_{\mathrm{cy}_{i,j-1}}^{\sigma^k}+D_{\mathrm{cy}_{i,j}}^{\sigma^k}\right)c_{i,j-1}^{k+1}$$
$$=\frac{r}{4}\left(D_{\mathrm{cx}_{i,j}}^{\sigma^k}+D_{\mathrm{cx}_{i-1,j}}^{\sigma^k}\right)c_{i-1,j}^{k+1/2}+\left[1+\frac{\Delta t}{2}J-\frac{r}{4}\left(D_{\mathrm{cx}_{i-1,j}}^{\sigma^k}+2D_{\mathrm{cx}_{i,j}}^{\sigma^k}+D_{\mathrm{cx}_{i+1,j}}^{\sigma^k}\right)\right]c_{i,j}^{k+1/2}+\frac{r}{4}\left(D_{\mathrm{cx}_{i,j}}^{\sigma^k}+D_{\mathrm{cx}_{i+1,j}}^{\sigma^k}\right)c_{i+1,j}^{k+1/2} \quad (27)$$

(i, j=1, 2, ..., M-1; k=0, 1, 2, ..., K-1)

4.3 Iterative solutions of the distribution of sulfate ion concentration

According to Eqs. (25) and (27), the iterative scheme of solutions to Eq. (1) is obtained by

$$\begin{cases}\left\{c_j^{k+1/2}\right\}=\left[\mathrm{A}'\right]^{-1}\left[B'\left\{c_{j-1}^{k}\right\}+C'\left\{c_{j+1}^{k}\right\}+D'\left\{c_j^{k}\right\}+\left\{e'\right\}\right]\\ \left\{c_i^{k+1}\right\}=\left[\mathrm{A}''\right]^{-1}\left[B''\left\{c_{i-1}^{k+\frac{1}{2}}\right\}+C''\left\{c_{i+1}^{k+\frac{1}{2}}\right\}+D''\left\{c_i^{k+\frac{1}{2}}\right\}+\left\{e''\right\}\right]\end{cases} \quad (28)$$

Where $\{c_j^{k+1/2}\}$ refers to M×1 order vector, which represents the concentrations of sulfate ions at every point $(x_i, y_j)_{(i=1,2,\ldots,M)}$ and time $t_{k+1/2}$; $\{c_i^{k+1}\}$ refers to N×1 order vector, which is the concentration of sulfate ions at every point $(x_i, y_j)_{(j=1,2,\ldots,N)}$ and time t_{k+1}. The other matrix and vectors in Eq. (28) are presented in the studied work (Zuo *et al.* 2017).

Table 1 List of main parameters used in the models (Zheng *et al.* 2012, Zuo *et al.* 2012a, b)

Parameter	Value	Parameter	Value	Parameter	Value	Parameter	Value
$L_1\times L_2$ (mm×mm)	400×400	f_{c0} (MPa)	26.8	D_{c}^{σ} (m^2/s)	2.62×10^{-12}	A_g	10.2
k_{v} (m^3/s/mol)	3.05×10^{-7}	f_{t0} (MPa)	2.68	x^{p}	0.0012	B_g	0.497
c_{Ca} (mol/m^3)	21.25	f_{e0} (MPa)	14.7	q_{c0}	0.55	A_c	1.995
c_0 (mol/m^3)	69	E_0 (MPa)	3.24×10^4	$\varepsilon_{\mathrm{c0}}^{\mathrm{d}}$	0.002	B_c	0.553

4.4 Numerical solution of time-varying stress in the prism section

Eq. (28) can be used to calculate the concentration of sulfate ion $c_{i,j}^{\ k}$ at the position (x_i, y_j) and time t_k , establish the corrosion front position $(x_{\mathrm{ch}}, y_{\mathrm{ch}})^k$ and the initial corrosion time $t_{0\mathrm{soi},j}$ of the position (x_i, y_j) in the prism cross section by Eq. (5), and to further calculate the corrosion time $t_{\mathrm{ini},j}^{\ k}$ of the position (x_i, y_j), using Eq. (6). Substituting $c_{i,j}^{\ k}$ and $t_{\mathrm{ini},j}^{\ k}$ into Eq. (4), the chemical damage degrees, $d_{\mathrm{c}i,j}^{\ k}$, can be obtained. So, the time-varying tensile and compressive strengths $f_{\varsigma i,j}^{k}$ and elastic modulus $E_{\varsigma i,j}^{k}$ of concrete are calculated from Eqs. (7) and (8).

To calculate the time-varying stress $\sigma_{\varsigma i,j}^{k}$ in the cross section of concrete prism under coupled axial force N and sulfate attack, firstly, Eq. (20) should be discretized by

$$N=\sum_{\mathrm{e}=1}^{\mathrm{M}\times\mathrm{N}}\sigma_{i,j}^{k}\cdot A_{\mathrm{e}} \quad (29)$$

Where e is the mesh element in the prism section, and A_{e} is the area of mesh element. However, $\sigma_{\varsigma i,j}^{k}$ calculated by the chemo-mechanical damage model, which can be numerical solved by the Euler backward algorithm (Zeng *et al.* 1996), should satisfy Eq. (29). Also, the capacity $N_{u\varsigma}^{k}$ of concrete prism should be equal or greater than the external load N, which can be calculated by

$$N_{\mathrm{u}\varsigma}^{k}=\sum_{\mathrm{e}=1}^{\mathrm{M}\times\mathrm{N}}f_{\varsigma i,j}^{\ k}\cdot A_{\mathrm{e}} \quad (30)$$

Finally, a computer program is written to analyze the time-varying stress in the concrete prism by using MATLAB language and the schematics of calculation flow are shown in Fig. 5.

5. Numerical example

5.1 Model parameters

The size of study object-concrete prism is 400 mm×400 mm ($L_1\times L_2$), in which the ordinary Portland cement and sodium sulfate solution with a concentration of 69 mol/m^3 were used. Due to the symmetry of the sulfate ion diffusion in the concrete specimen, a quarter section with 200 mm×200 mm was selected to simplify the calculation. Some calculation parameters in the above models, including the mechanical parameters of concrete, diffusion-reaction and damage parameters, are listed in Table 1.

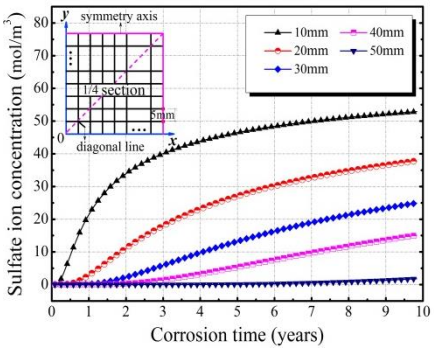

(a) With the corrosion time

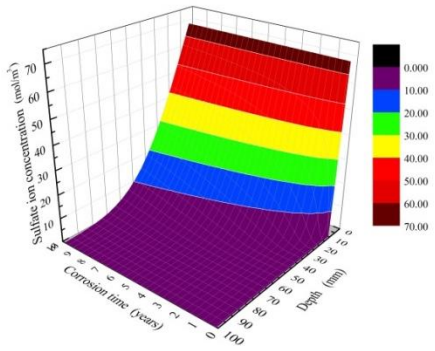

(b) With the depth and corrosion time

Fig. 6 Changes of sulfate ion concentration in the direction of the symmetry axis of prism section

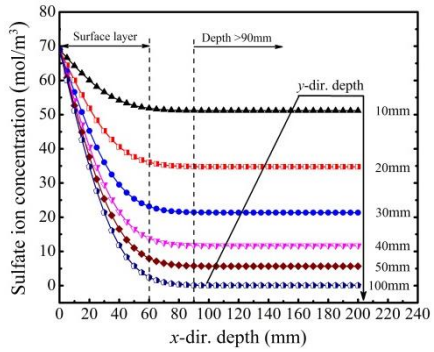

(a) At *x*-dir. depth

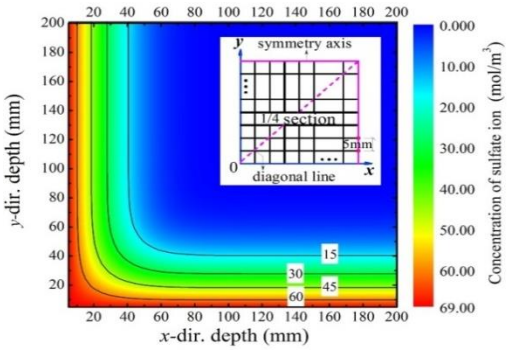

(b) At *x*- and *y*-dir. depth

Fig. 7 Distribution of sulfate ion concentration in concrete after corrosion for 8 years

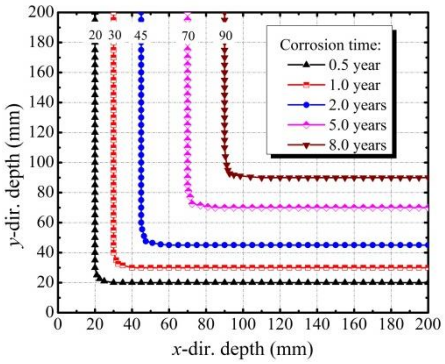

Fig. 8 Corrosion depth at different corrosion time

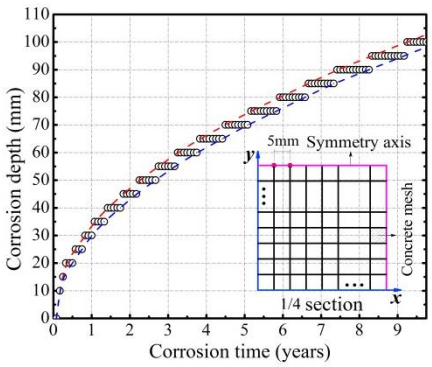

Fig. 9 Change of corrosion depth in the direction of the symmetry axis with corrosion time

5.2 Numerical results

5.2.1 Sulfate ion concentration

Fig. 6 shows the changes of sulfate ion concentration in the direction of the symmetry axis with the surface depth and corrosion time, while Fig. 7 presents the distribution of sulfate ion concentration in the concrete subjected to sulfate attack for 8 years. It can be seen from Fig. 6 that, the sulfate ion concentration increases with corrosion time at different surface depths, but its increasing rate gradually decrease with the surface depth, which indicates a great gradient distribution of sulfate ion concentration at the surface layer (0-60 mm). However, in the interior of the specimen section, the sulfate ion concentration has a low gradient distribution, and has basically no change at greater depths (>90 mm), as shown in Fig. 6(b) and Fig. 7. This is because, after corrosion for a period of time, the diffusion rate of sulfate ion in concrete is equal to its consumption rate caused by chemical reactions in Eq. (2), so there is a dynamic equilibrium between the diffusion and reaction of sulfate ion in concrete (Zuo *et al.* 2012b). In addition, Fig. 7(b) gives the isolines of sulfate ion concentration, the shape of which is consistent with the studied results (Tixier *et al.* 2003).

5.2.2 Corrosion depth

In the diffusion process of sulfate ion from the surface to the interior of concrete, the corrosion depth can be characterized by the position of the sulfate-corroded front, as defined in Eq. (5), so the initial corrosion time is that of

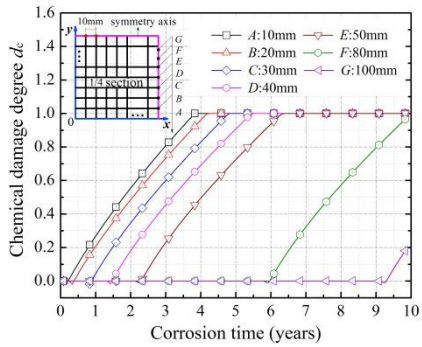

(a) With corrosion time

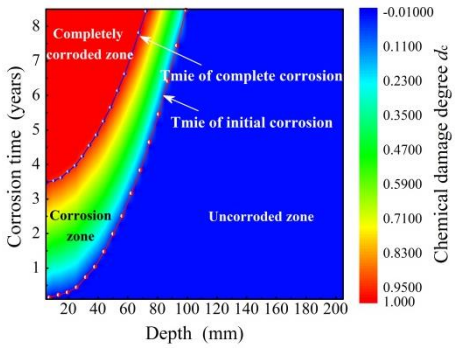

(b) With the depth and corrosion time

Fig. 10 Changes of chemical damage degree d_c with the depth and corrosion time

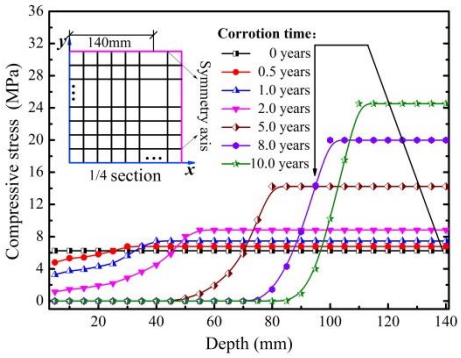

Fig. 11 Changes of compressive stress with the depth

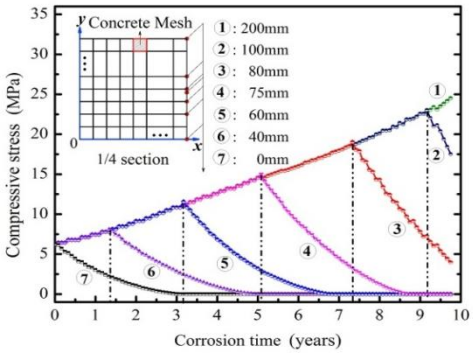

Fig. 12 Changes of compressive stress in symmetry in the direction of symmetry axis with the corrosion time

sulfate ion diffusing into the front position, which can be obtained by numerical solution, satisfied by Eq. (5). The corrosion depth at different corrosion times is presented by Fig.8. It can be seen from the figure that the corrosion depth has a gradual increase with the corrosion time, and the shapes of these isolines formed by the depths at same corrosion time are identical to that of sulfate ion concentration shown in Fig. 7(b). Fig. 9 shows the changes of the corrosion depth in the direction of the symmetry axis with the corrosion time. It can be observed from Fig. 9 that, the corrosion depth undergoes rapid increase at the initial corrosion stage, but its increasing rate has a gradual decrease with the corrosion time. Also from Fig. 9, the corrosion depth in the direction of the symmetry axis reaches about 6.5 cm after corrosion for first 4 years, but only increased by 2.5 cm for the next 4 years of corrosion.

5.2.3 Chemical damage

Fig. 10 presents the changes of the chemical damage degree d_c, calculated by Eqs. (1), (4) and (6), in the direction of the symmetry axis with the depth and corrosion time. It can be seen from Fig. 10 that, the damage degree at the surface layer of concrete has an obvious increase at the initial stage of sulfate attack, and its strength has a complete loss after corrosion for 3.5 years. However, the time interval between initial damage of concrete and complete loss of its strength has a gradual increase with the surface depth. For example, they are respectively 4.00- and 4.16-years at the positions 20 mm and 50 mm in the direction of symmetry axis. This is because, the concentration of sulfate ion in the interior of prism is lower than that at the surface layer, so it requires more time for complete degradation of the interior concrete, known from Eq. (4). In addition, the curves of initial corrosion time and complete corrosion time are marked to distinguish the uncorroded zone (d_c=0), the corrosion zone (0<d_c<1), and the completely corroded zone (d_c=1), as shown in Fig. 10(b).

5.2.4 Stress redistribution

An axial compression of 1000 kN was applied to the two ends of the prism to investigate the stress redistribution of concrete in the process of sulfate attack. Fig. 11 presents the changes of the compressive stress with the depth in the direction of the symmetry axis. It can be seen from the figure that, the distribution curve of compressive stresses in the uncorroded concrete prism (0 year) is a straight line, and equal to 6.25 MPa. With the increasing of corrosion time, the compressive stresses in the corroded zone of the section has a gradual decrease, but has an increase in the uncorroded zone, and so its distributed gradient has obvious increase from the interior to the surface of the prism, which is called as the phenomenon of stress redistribution, and it is attributed to the deterioration of elastic modulus of concrete (Idiart *et al.* 2011, Lee *et al.* 2008) and the increment of the corroded zone in the section of prism caused by sulfate attack, as shown in Fig. 10(b). Thus, the concrete in uncorroded zone bears a higher proportion of axial compression, resulting in the increase of its compressive stress.

In the direction of the symmetry axis of the prism

section, the changes of the compressive stress with corrosion time is illustrated in Fig. 12. It can be seen from the figure that, at different depth of concrete prism, the compressive stress has almost linear increase at the initial corrosion stage, and then begins to produce an obvious decrease, here, except for the compressive stress at the depth of 200 mm, and its decreasing rate slows down with the corrosion time. The inflection point in the curve of compressive stress in Fig. 12, is attributed to the reduction of elastic modulus of concrete caused by sulfate attack. The time corresponding to inflection point is the initial corrosion time of concrete. For example, the initial corrosion time at the depth of 60 mm (stress curve 5) is 3.15 years.

6. Conclusions

In the process of sulfate attack on concrete, the changes of stress in concrete caused axial loading with corrosion time is modeled, which mainly includes the diffusion and reaction of sulfate ion, chemical damage and the stress redistribution induced by the chemo-mechanical damage. Numerical simulation on an axially compressed concrete prism immersed into sulfate solution has been carried out to investigate the time-varying stress in concrete, and the main conclusions are as follows:

• The concentration of sulfate ion in concrete increases with corrosion time, but decreases with the increasing of corrosion depth, and it has a great gradient distribution at the surface layer of concrete.

• The corrosion depth in concrete has an obvious increase at the initial corrosion stage, but its increasing rate has a gradual decrease with the corrosion time.

• The chemical damage degree of concrete is related to the distribution of sulfate ion concentration in concrete, and it increases with the sulfate ion concentration. Moreover, there has a great gradient distribution of chemical damage degree in the corroded zone.

• Before sulfate attack, the stress in the axially compressed concrete has a uniform distribution. But, after sulfate corrosion for a period of time, the corroded zone in the section extends inward and the chemical damage degree has a continual increase with the corrosion time. The stress decreases in the corroded zone and increase in the uncorroded zone.

Acknowledgments

This study was financially supported by National Science Foundation of China (51378262, 51078186) and Jiangsu Province Science Foundation (BK20141396).

References

Bassuoni, M.T. and Nehdi, M.L. (2009), "Durability of self-consolidating concrete to sulfate attack under combined cyclic environments and flexural loading", *Cement Concrete Res.*, **39**(3), 206-226.

Cao, S. (1991), "Mechanical properties of corroded concrete", *J. Southeast Univ.*, **21**(4), 89-95.

Etse, G. and Willam, K. (1999), "Failure analysis of elastoviscoplastic material models", *J. Eng. Mech.*, **125**(1), 60-69.

Faria, R., Oliver, J. and Cervera, M. (1998), "A strain-based plastic viscous-damage model for massive concrete structures", *J. Solids Struct.*, **35**(14), 1533-1558.

Gao, J., Yu, Z., Song, L., Wang, T. and Wei, S. (2013), "Durability of concrete exposed to sulfate attack under flexural loading and drying-wetting cycles", *Constr. Build. Mater.*, **39**, 33-38.

Grassl, P. and Jirásek, M. (2006), "Damage-plastic model for concrete failure", *J. Solids Struct.*, **43**(22-23), 7166-7196.

Grassl, P., Lundgren, K. and Gylltoft, K. (2002), "Concrete in compression: A plasticity theory with a novel hardening law", *J. Solids Struct.*, **39**(20), 5205-5223.

Güneyisi, E., Gesoğlu, M. and Mermerdaş, K. (2010), "Strength deterioration of plain and metakaolin concretes in aggressive sulfate environments", *J. Mater. Civil Eng.*, **22**(4), 403-407.

Idiart, A.E., López, C.M. and Carol, I. (2011), "Chemo-mechanical analysis of concrete cracking and degradation due to external sulfate attack: A meso-scale model", *Cement Concrete Compos.*, **33**(3), 411-423.

Kalipcilar, I., Mardani, A., Sezer A. and Altun, S. (2016), "Assessment of the effect of sulfate attack on cement stabilized montmorillonite", *Geomech. Eng.*, **10**(6), 807-826.

Lee, S.T., Hooton, R.D., Jung, H., Park, D. and Choi, C.S. (2008), "Effect of limestone filler on the deterioration of mortars and pastes exposed to sulfate solutions at ambient temperature", *Cement Concrete Res.*, **38**(1), 68-76.

Liang, Y.N. and Yuan, Y.S. (2005), "Effects of environmental factors of sulfate attack on deterioration of concrete mechanical behavior", *J. China Univ. Min. Technol.*, **34**(4), 452-457.

Liu, T., Zou, D., Teng, J. and Yan, G. (2012b), "The influence of sulfate attack on the dynamic properties of concrete column", *Constr. Build. Mater.*, **28**(1), 201-207.

Liu, Z., Deng, D., Schutter, G.D. and Yu, Z. (2012a), "Chemical sulfate attack performance of partially exposed cement and cement+fly ash paste", *Constr. Build. Mater.*, **28**(1), 230-237.

Lubliner, J., Oliver, J., Oller, S. and Oñate, E. (1989), "A plastic-damage model for concrete", *J. Solids Struct.*, **25**(3), 299-326.

Mazars, J. and Pyaudier-Cabot, G. (1989), "Continuum damage theory-application to concrete", *J. Eng. Mech.*, **115**(2), 345-365.

Menetrey, P. and Willam, K. (1995), "Triaxial failure criterion for concrete and its generalization", *ACI Struct. J.*, **92**(3), 311-318.

Nehdi, M.L., Suleiman, A.R. and Soliman, A.M. (2014), "Investigation of concrete exposed to dual sulfate attack", *Cement Concrete Res.*, **64**, 42-53.

Neville, A. (2004), "The confused world of sulfate attack on concrete", *Cement Concrete Res.*, **34**(8), 1275-1296.

Nie, Q., Zhou, C., Li, H., Shu, X., Gong, H. and Huang, B. (2015), "Numerical simulation of fly ash concrete under sulfate attack", *Constr. Build. Mater.*, **84**, 261-268.

Saetta, A., Scotta, R. and Vitaliani, R. (1998), "Mechanical behavior of concrete under physical-chemical attacks", *J. Eng. Mech.*, **124**(10), 1100-1109.

Samson, E. and Marchand, J. (2007), "Modeling the transport of ions in unsaturated cement-based materials", *Comput. Struct.*, **85**(23-24), 1740-1756.

Santhanam, M., Cohen, M.D. and Olek, J. (2003), "Effects of gypsum formation on the performance of cement mortars during external sulfate attack", *Cement Concrete Res.*, **33**(3), 325-332.

Sarkar, S., Mahadevan, S., Meeussen, J.C.L., Sloot, H.V.D. and Kosson, D.S. (2010), "Numerical simulation of cementitious materials degradation under external sulfate attack", *Cement Concrete Compos.*, **32**(3), 241-252.

Schneider, U. and Chen, S.W. (1998), "Modeling and empirical formulas for chemical corrosion and stress corrosion of

cementitious materials", *Mater. Struct.*, **31**(10), 662-668.
Shao, J.F., Jia, Y., Kondo, D. and Chiarelli, A.S. (2006), "A coupled elastoplastic damage model for semi-brittle materials and extension to unsaturated conditions", *Mech. Mater.*, **38**(3), 218-232.
Sun, C., Chen, J., Zhu, J., Zhang, M. and Ye, J. (2013), "A new diffusion model of sulfate ions in concrete", *Constr. Build. Mater.*, **39**, 39-45.
Sun, W. and Zuo, X.B. (2012), "Numerical simulation of sulfate diffusivity in concrete under combination of mechanical loading and sulfate environments", *J. Sustain. Cement-Based Mater.*, **1**(1-2), 46-55.
Taqieddin, Z.N., Voyiadjis, G.Z. and Almasri, A.H. (2012), "Formulation and verification of a concrete model with strong coupling between isotropic damage and elastoplasticity and comparison to a weak coupling model", *J. Eng. Mech.*, **138**(5), 530-541.
Taylor, H.F.W., Famy, C. and Scrivener, K.L. (2001), "Delayed ettringite formation", *Cement Concrete Res.*, **31**(5), 683-693.
Tixier, R. and Mobasher, B. (2003), "Modeling of damage in cement-based materials subjected to external sulfate attack. I: Formulation", *J. Mater. Civil Eng.*, **15**(4), 305-313.
Wu, J.Y., Li, J. and Faria, R. (2006), "An energy release rate-based plastic-damage model for concrete", *J. Solids Struct.*, **43**(3-4), 583-612.
Xiong, C.S., Jiang, L.H., Zhang, Y. and Chu, H.Q. (2015), "Modeling of damage in cement paste subject to external Sulfate attack", *Comput. Concrete*, **16**(6), 847-864.
Yang, D.Y., We, S.N. and Tan, Y.Q. (2005), "Performance evaluation of binary blends of portland cement and fly ash with complex admixture for durable concrete structures", *Comput. Concrete*, **2**(5), 381-388
Yuan, J., Liu, Y., Tan, Z.C. and Zhang, B.K. (2016), "Investigating the failure process of concrete under the coupled actions between sulfate attack and drying-wetting cycles by using x-ray CT", *Constr. Build. Mater.*, **108**, 129-138.
Yu, Y., Zhang, Y.X. and Khennane, A. (2015), "Numerical modelling of degradation of cement-based materials under leaching and external sulfate attack", *Comput. Concrete*, **158**, 1-14.
Yu, S.W. and Feng, X.Q. (1997), "Damage mechanics", Tsinghua University Press, Beijing, China.
Zeng, L.F., Horrigmoe, G. and Andersen, R. (1996), "Numerical implementation of constitutive integration for rate-independent elastoplasticity", *Comput. Mech.*, **18**(5), 387-396.
Zheng, F.G., Wu, Z., Gu, C., Bao, T. and Hu, J. (2012), "A plastic damage model for concrete structure cracks with two damage variables", *Sci. China Technol. Sci.*, **55**(11), 2971-2980.
Zhou, Y., Li, M., Sui, L. and Xing, F. (2016), "Effect of sulfate attack on the stress-strain relationship of FRP-confined concrete", *Constr. Build. Mater.*, **110**, 235-250.
Zuo, X.B., Sun, W., Li, H. and Zhao, Y.K. (2012a), "Modeling of diffusion-reaction behavior of sulfate ion in concrete under sulfate environments", *Comput. Concrete*, **10**(1), 47-51.
Zuo, X.B., Sun, W., Yu, C. and Wan, X.R. (2010), "Modeling of ion diffusion coefficient in saturated concrete", *Comput. Concrete*, **7**(5), 421-435.
Zuo, X.B., Sun, W. and Yu, C. (2012b), "Numerical investigation on expansive volume strain in concrete subjected to sulfate attack", *Constr. Build. Mater.*, **36**(4), 404-410.
Zuo, X.B., Wang, J.L., Sun, W., Li, H. and Yin, G.J. (2017), "Numerical investigation on gypsum and ettringite formation in cement pastes subjected to sulfate attack", *Comput. Concrete*, **19**(1), 19-31.